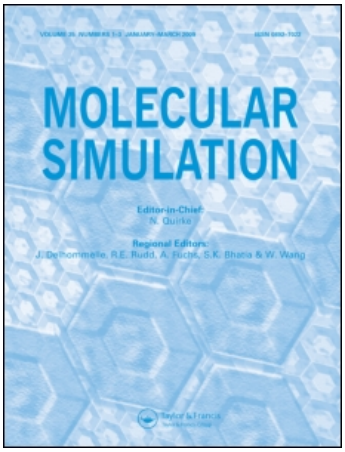

Molecular Simulation
Publication details, including instructions for authors and subscription information:
http://www.informaworld.com/smpp/title~content=t713644482

Phonon interactions in zeolites mediated by anharmonicity and adsorbed molecules

Chia-Yi Chen[a]; Dmitry I. Kopelevich[a]
[a] Department of Chemical Engineering, University of Florida, Gainesville, USA

To cite this Article Chen, Chia-Yi and Kopelevich, Dmitry I.(2008) 'Phonon interactions in zeolites mediated by anharmonicity and adsorbed molecules', Molecular Simulation, 34: 2, 155 — 167
To link to this Article: DOI: 10.1080/08927020802036070
URL: http://dx.doi.org/10.1080/08927020802036070

Molecular Simulation
Vol. 34, No. 2, February 2008, 155–167

Taylor & Francis
Taylor & Francis Group

Phonon interactions in zeolites mediated by anharmonicity and adsorbed molecules

Chia-Yi Chen and Dmitry I. Kopelevich*

Department of Chemical Engineering, University of Florida, Gainesville, USA

(Received 17 January 2008; final version received 24 February 2008)

There is increasing evidence that thermal conductivity of nanoporous materials can be significantly affected by adsorption of guest molecules. These molecules serve as moving defects and provide additional scattering centres for heat-carrying phonons. In order to understand the sorbate–phonon interactions, we perform molecular dynamics simulations of a model system, namely sodalite zeolite with small molecules (argon, xenon and methane) encapsulated in its cages. We measure effects of sorbates on several important characteristics of phonon dynamics, such as correlations between different phonon modes and the phonon frequency and lifetime. The dominant effect of the sorbate–phonon interactions is observed to be a change of phonon lifetime. The phonon lifetime often increases upon encapsulation of a sorbate into the zeolite which suggests that the sorbate–phonon interactions are qualitatively different from phonon scattering by point defects fixed in the lattice.

Keywords: phonons; nanoporous materials; sorbates; nonlinear dynamics

1. Introduction

Zeolites are microporous alumino-silicate crystals with pore sizes comparable to molecular dimensions. They are widely used as molecular sieves, sorbents, catalysts and ion exchangers. In addition, several possible applications of zeolites combining adsorption of guest molecules with temperature control are emerging. Examples include solar adsorption heat pump [1] and adsorption chillers for microelectronic devices [2].

A wide variety of available zeolite structures provides a large range of flexibility in fine-tuning their thermal properties to a specific task. Zeolite thermal conductivity can also be altered by introducing point defects into the crystal lattice, e.g. by substitution of some of the silicon atoms by aluminum [3]. The point defects provide additional scattering centres for phonons thus reducing the crystal thermal conductivity [4]. Moreover, the nanoporous structure of zeolites provides an additional opportunity to control the zeolite thermal properties through introduction of off-framework guest species (sorbates or cations) into the crystal. In fact, it is well known that strong interaction between zeolite lattice vibrations and guest molecules significantly affects transport properties of the guest molecules [5–7] as well as the dynamics of oscillation of sorbate molecules at their adsorption sites [8]. Evidence is accumulating that the presence of guest molecules within zeolites also affects the dynamics of zeolite lattice vibrations leading to changes in thermal properties of zeolites [9,10].

Similar host–guest interactions play a significant role in thermal conductivity of other nanoporous materials of technological importance. For example, skutterudites are promising candidates for development of efficient thermoelectric materials, i.e. materials with high ratio of electrical and thermal conductivities. It has been shown [11,12] that addition of ions to voids in skutterudites leads to an order of magnitude decrease of their thermal conductivity thus increasing the thermoelectric figure of merit.

Available data suggest complex dependence of the thermal conductivity on the nature of a guest molecule and a host crystal. As discussed above, addition of ions to skutterudites reduces their thermal conductivity. Similarly, encapsulation of an atom in a Ge clathrate leads to an order of magnitude reduction in thermal conductivity [13]. In addition, molecular dynamics (MD) simulations [9] show a drastic reduction of thermal conductivity of zeolite LTA–SiO_2 in the presence of heavy cations. These results seem to suggest that 'rattling' of the guest species inside a crystal leads to scattering of phonons thus reducing their mean free path and leading to the decrease of thermal conductivity.

However, other observations contradict this picture. For example, MD simulations of xenon in zeolite LTA–SiO_2 indicate an increase of the zeolite thermal conductivity due to the guest–host interactions [9]. In addition, experiments of Greenstein et al. [10] show that the conductivity of zeolite MFI is substantially higher

*Corresponding author. Email: dkopelevich@che.ufl.edu

ISSN 0892-7022 print/ISSN 1029-0435 online

DOI: 10.1080/08927020802036070
http://www.informaworld.com

when an organic template cation tetrapropylammonium is present in it, as compared to a sample with removed templates.

Therefore, the phonon–guest interactions may be qualitatively different from the phonon scattering by point defects fixed in the lattice due to strongly nonlinear oscillations of guest molecules inside the crystal pores. Interactions of guest molecules with host lattice vibrations have been extensively modelled in recent years [7,8,14–16]. Typically, the goal of these studies is to understand the effects of the lattice vibration on the sorbate dynamics inside crystals and the lattice vibrations are frequently modelled as a thermal bath. In the current work, we are aiming to understand the reverse process, i.e. the effects of the sorbate 'rattling' on the crystal lattice vibrations. In this paper, we present results of our investigations of the effects of sorbate molecules on dynamics of individual phonons. It is expected that an understanding of sorbate–phonon interactions will lead to a better understanding of the sorbate effects on thermal conductivity of nanoporous materials. We consider a relatively simple system, namely a sodalite zeolite with small molecules (argon, xenon or methane) trapped inside its cages. Forces between these sorbates and zeolite lattice atoms are short-ranged and, when the sorbate size is sufficiently small, the interaction between the sorbate and the phonons takes place only during collisions between the sorbate and the zeolite wall. Therefore, the current model allows us to focus on effects of the sorbate 'rattling' on the phonon dynamics and our observations are not obscured by other possible contributions of guest molecules to the lattice dynamics, such as long-range electrostatic interactions between adsorbed charged species and lattice ions.

2. Model details

The crystal structure of silica sodalite $Si_{12}O_{24}$ is shown in Figure 1. This zeolite possesses a cubic symmetry and its lattice parameter is 8.83 Å [17]. A sodalite unit cell consists of a cage shaped like a truncated cuboctahedron bounded by six 4-ring windows (i.e. windows formed by four oxygen and four silicon atoms) and eight 6-ring windows. Diameter of the 4-ring windows is very small and these windows are impermeable by the sorbates considered in our simulations. In addition, transport rates of argon and larger molecules (methane and xenon) through the 6-ring windows are orders of magnitude slower than the phonon–phonon and phonon–sorbate interactions [6] and a sorbate remains inside a cage on the time-scale of interest.

Silica sodalite is usually synthesised by growing the crystal around organic template molecules which become encapsulated in the sodalite cages after the synthesis is complete [17,18]. In the current work, we neglect the presence of encapsulated templates and perform MD simulations of either bare silica sodalite containing only Si and O atoms in its lattice structure or silica sodalite with encapsulated argon, methane or xenon molecules.

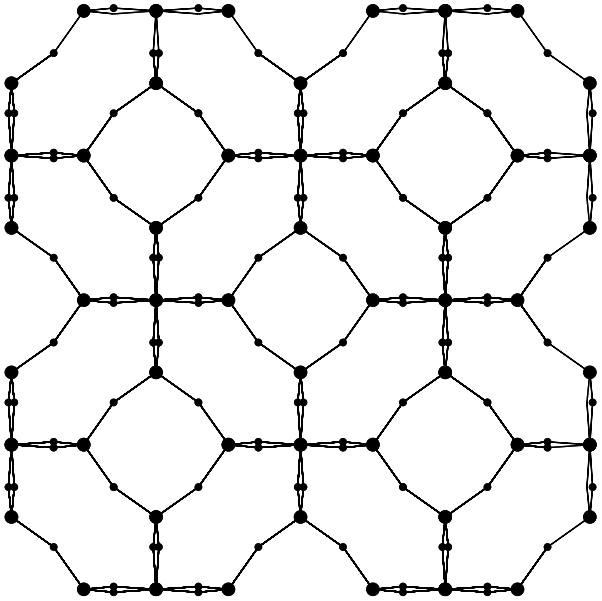

Figure 1. A block of 2 × 2 × 2 sodalite unit cells containing nine sodalite cages. Silicon and oxygen atoms are shown as larger and smaller spheres, respectively. In MD simulations of sorbate–lattice systems, the sorbates are located in eight corner cages of this block.

The equilibrium lattice configuration and the potential model for zeolite lattice vibrations used in this study are the same as those used by Kopelevich and Chang [6] in a study of sorbate transport through 6-ring windows. Zeolite lattice vibrations are modelled by a truncated version of an anharmonic potential energy field proposed by Nicholas et al. [19],

$$V = \sum_{\mathrm{O—Si}} V_r(r^{\mathrm{O—Si}}) + \sum_{\mathrm{O—Si—O}} V_\alpha(\alpha^{\mathrm{O—Si—O}}) + \sum_{\mathrm{Si—O—Si}} [V_\beta(\beta^{\mathrm{Si—O—Si}}) + V_{\mathrm{UB}}(r^{\mathrm{Si—Si}})], \quad (1)$$

where

$$V_r(r) = \frac{1}{2} K_r \left(r - r_0^{\mathrm{O—Si}}\right)^2, \quad (2)$$

is the potential energy of stretching of the O—Si bond r,

$$V_\alpha = \frac{1}{2} K_\alpha (\alpha - \alpha_0)^2, \quad (3)$$

is the potential energy of bending of the O—Si—O bond angle α,

$$V_\beta = \frac{1}{2}\left[K_\beta^{(1)}(\beta-\beta_0)^2 - K_\beta^{(2)}(\beta-\beta_0)^3 + K_\beta^{(3)}(\beta-\beta_0)^4\right], \tag{4}$$

is the potential energy of bending of the Si—O—Si bond angle β, and

$$V_{\mathrm{UB}}(r) = \frac{1}{2}K_{\mathrm{UB}}\left(r - r_0^{\mathrm{Si-Si}}\right)^2, \tag{5}$$

is the Urey-Bradley term which represents lengthening of the Si—O bond as the Si—O—Si angle becomes smaller. In (5), r denotes distance between two silicon atoms of a Si—O—Si angle.

The potential model (1) neglects smaller contributions included in the original model [19] such as torsion energy of the dihedral Si—O—Si—O angle, nonbonded Lennard-Jones interaction and electrostatic interaction between zeolite atoms due to the partial charges of Si and O atoms. In principle, long-range electrostatic interactions may have a significant effect on the lattice dynamics. However, it has been shown in [19] that electrostatic interactions have little effect on the structure or dynamics of the silica sodalite lattice due to high symmetry of this crystal and charge neutrality of each SiO_2 group. Moreover, since the sorbates considered in the current work are electrically neutral, electrostatic interactions with the partial charges of the lattice atoms are expected to have negligible effects on the sorbate dynamics. In fact, this truncated model has been shown to yield good agreement between computed and experimental values of transport rates of inert gases in sodalite [6]. Since this transport process involves large deformations of 6-ring windows, it is expected that, despite the introduced approximations, the model (1) will provide an accurate description of anharmonic lattice dynamics.

The values of the force constants K as well as the values of the equilibrium distances ($r_0^{\mathrm{O-Si}}$ and $r_0^{\mathrm{Si-Si}}$) and equilibrium bond angles α_0 and β_0 are summarised in Table 1. The force constants and the equilibrium bond angles were taken from the paper of Nicholas et al. [19]. The equilibrium distances $r_0^{\mathrm{Si-Si}}$ and $r^{\mathrm{O-Si}}$ were obtained from a requirement that the equilibrium crystal structure predicted by the potential field should coincide with the structure obtained experimentally by Richardson et al. [17]. The value of $r_0^{\mathrm{O-Si}}$ used in this work is somewhat different from that proposed by Nicholas et al. [19] due to the differences in the potential as discussed in detail in [6].

Table 1. Parameters for the lattice potential energy model (1).

Si—O	$K_r = 2500.1\,\mathrm{kJ\,mol^{-1}\,\AA^{-2}}$	$r_0^{\mathrm{O-Si}} = 1.58\,\AA$
O—Si—O	$K_\alpha = 578.1\,\mathrm{kJ\,mol^{-1}\,rad^{-2}}$	$\alpha_0 = 109.5°$
Si—O—Si	$K_\beta^{(1)} = 45.4\,\mathrm{kJ\,mol^{-1}\,rad^{-2}}$	$\beta_0 = 149.5°$
	$K_\beta^{(2)} = 95.1\,\mathrm{kJ\,mol^{-1}\,rad^{-3}}$	
	$K_\beta^{(3)} = 55.5\,\mathrm{kJ\,mol^{-1}\,rad^{-4}}$	
Si—Si	$K_{\mathrm{UB}} = 228.5\,\mathrm{kJ\,mol^{-1}\,\AA^{-2}}$	$r_0^{\mathrm{Si-Si}} = 3.1219\,\AA$

In order to assess sorbate size effects on the phonon–sorbate interactions, we consider three different sorbates, namely argon, methane and xenon. All these sorbates are modelled as spheres which interact with each other and the zeolite lattice atoms through the Lennard-Jones potential. The values of the Lennard-Jones parameters ε and σ used in our calculations are listed in Table 2. The sorbate–lattice interactions are modelled using the common assumptions [20] that the interaction between sorbates and lattice silicon atoms can be neglected and that the only contribution to the sorbate–lattice potential energy is due to interaction between sorbates and lattice oxygen.

3. Simulation details

The simulations were performed at temperature $T = 300\,\mathrm{K}$ for a $2 \times 2 \times 2$ block of sodalite unit cells satisfying the periodic boundary conditions. Initial configurations for the simulations were prepared as follows. First, sorbate-free zeolite was considered. Initial conditions were generated by placing zeolite atoms at their equilibrium positions and sampling their velocities from the Maxwell distribution. The bare zeolite lattice was then equilibrated for 10 ns using NVT (constant number of particles, volume and temperature) simulations with Berendsen thermostat [21] with the time constant 1 ps.

After this equilibration, one or more sorbate molecules were added to each of the corner cage of the $2 \times 2 \times 2$ sodalite block (Figure 1) and the sorbate–lattice system was equilibrated using the NVT simulations for an additional 2 ns. The initial locations for the sorbates were taken to correspond to the minimum of the sorbate–zeolite potential energy. Due to the small size of the sodalite cages, only one xenon molecule and no more than two argon or methane molecules can be placed into a single cage. Therefore, we consider the following five sorbate–lattice systems: one sorbate (Ar, CH_4 or Xe) per unit cell and two sorbates (Ar or CH_4) per unit cell.

Table 2. Lennard-Jones parameters for sorbate–sorbate and sorbate–lattice interactions.

Interaction	ϵ (J/mol)	σ (Å)
Ar–Ar [29]	1183.0	3.350
Ar–O [29]	1028.0	3.029
CH_4–CH_4 [30]	1139.0	3.882
CH_4–O [31]	1108.3	3.214
Xe–Xe [29]	3437.0	3.849
Xe–O [32]	1133.1	3.453

We will denote these systems as 1 Ar/cage, 1 CH_4/cage, 1 Xe/cage, 2 Ar/cage and 2 CH_4/cage.

The equilibration was followed by a 5 ns production run of NVE (constant number of particles, volume and energy) simulations for each of these five sorbate–lattice systems and the sorbate-free zeolite. Since one of the main goals of this work is to assess chaotic nonlinear dynamics of phonons, we chose a fairly small step size, $\Delta t = 0.1$ fs, for the microcanonical simulations. This step size ensures that the total energy fluctuations are on the order of 0.001%.

In order to demonstrate that the sorbate 'rattling' inside the zeolite cage is qualitatively different from harmonic or nearly harmonic oscillations of point defects in the lattice, we performed additional simulations of sorbate dynamics in the absence of the sorbate–phonon interactions. In these simulations, the zeolite atoms were fixed at their equilibrium positions. The sorbates were initially placed at positions corresponding to the minimum of the sorbate–zeolite potential energy and their velocity was sampled from the Maxwell distribution. The system was then equilibrated for 2 ns using the NVT simulations, which were followed by a 5 ns NVE production run. The parameters of these NVT and NVE simulations are the same as those of the simulations of the flexible zeolite systems.

4. Normal modes of sodalite crystal

Before presenting analysis of our MD simulations in Sections 5 and 6, we briefly review background information on harmonic lattice dynamics and calculation of sodalite normal modes.

Consider a crystal modelled by a periodically repeated block of $L_1 \times L_2 \times L_3$ unit cells. Each unit cell contains N atoms and two vector sets $\{\mathbf{a}_1, \mathbf{a}_2, \mathbf{a}_3\}$ and $\{\mathbf{b}_1, \mathbf{b}_2, \mathbf{b}_3\}$ form bases of the unit cell and the reciprocal lattice, respectively; $\mathbf{a_i}\cdot\mathbf{b_j} = 2\pi\delta_{ij}$.

Let integer vector $\mathbf{l} = (l_1, l_2, l_3)$ specify the unit cell with coordinates

$$\mathbf{r}(\mathbf{l}) = l_1\mathbf{a}_1 + l_2\mathbf{a}_2 + l_3\mathbf{a}_3, \quad l_i = 0, \ldots, L_i - 1. \tag{6}$$

In addition, let $\mathbf{r}(\mathbf{l}\kappa)$ denote the coordinates of the κth atom within the $\mathbf{l}$th unit cell and $\mathbf{u}(\mathbf{l}\kappa) = \mathbf{r}(\mathbf{l}\kappa) - \mathbf{r}^{\mathrm{eq}}(\mathbf{l}\kappa)$ denote displacement of this atom from its equilibrium position $\mathbf{r}^{\mathrm{eq}}(\mathbf{l}\kappa)$. Then, the normal mode coordinates $Q_{j\mathbf{k}}$ are defined as the projection of the Fourier transform of $\mathbf{u}(\mathbf{l}\kappa)$ on eigenvectors $\mathbf{e}(j\mathbf{k})$ of the Fourier transform $\mathbf{D}(\mathbf{k})$ of the dynamical matrix [22]. Here, j is a number of the eigenmode and $\mathbf{k}$ is a wavevector,

$$\mathbf{k} = \frac{h_1}{L_1}\mathbf{b}_1 + \frac{h_2}{L_2}\mathbf{b}_2 + \frac{h_3}{L_3}\mathbf{b}_3, \quad h_i = 0, \ldots, L_i - 1, \quad i = 1, 2, 3. \tag{7}$$

In what follows, we will use crystallographic notation for this vector, i.e. the right-hand side of Equation (7) will be written as $\mathbf{k} = [h_1 h_2 h_3]$.

Elements of the matrix $\mathbf{D}(\mathbf{k})$ are given by

$$D_{\alpha\beta}(\kappa\kappa';\mathbf{k}) = (m_\kappa m_{\kappa'})^{-1/2} \times \sum_{\mathbf{l}'} \left(\frac{\partial^2 V}{\partial r_\alpha(\mathbf{l}\kappa)\partial r_\beta(\mathbf{l}'\kappa')}\right)\Bigg|_{\mathbf{r}=\mathbf{r}^{\mathrm{eq}}} \mathrm{e}^{-i\mathbf{k}\cdot\mathbf{r}(\mathbf{l}-\mathbf{l}')}, \quad \alpha, \beta = 1, 2, 3, \quad \kappa, \kappa' = 1, \ldots, N. \tag{8}$$

Here, $\mathrm{m_k}$ is the mass of the k-th atom of a unit cell.

Solution of the eigenvalue problem for this $3N \times 3N$ matrix,

$$\sum_{\kappa'=1}^{N}\sum_{\beta=1}^{3} D_{\alpha\beta}(\kappa\kappa';\mathbf{k})e_\beta(\kappa';j\mathbf{k}) = \omega_{j\mathbf{k}}^2 e_\alpha(\kappa;j\mathbf{k}), \quad j = 1, \ldots, 3N, \tag{9}$$

yields frequencies $\omega_{j\mathbf{k}}$ of the normal mode vibrations.

The normal mode coordinates can now be defined as follows [22]

$$\mathrm{Q}_{j\mathbf{k}} = (L_1L_2L_3)^{-1/2} \times \sum_{\mathbf{l}}\sum_{\kappa=1}^{N}\sum_{\alpha=1}^{3} m_\kappa^{1/2} u_\alpha(\mathbf{l}\kappa)e_\alpha^*(\kappa;j\mathbf{k})\mathrm{e}^{-i\mathbf{k}\cdot\mathbf{r}(\mathbf{l})}. \tag{10}$$

In the case of a harmonic and sorbate-free lattice, the normal modes are independent of each other and the Hamiltonian of each mode is

$$H_{j\mathbf{k}} = \frac{1}{2}|\dot{Q}_{j\mathbf{k}}|^2 + \frac{1}{2}\left(\omega_{j\mathbf{k}}^h\right)^2|Q_{j\mathbf{k}}|^2. \tag{11}$$

Here and in the remainder of the paper, we use superscript h to distinguish frequency of a normal mode in a harmonic lattice from that in an anharmonic lattice.

The sodalite unit cell contains $N = 36$ atoms. Therefore, there are 108 normal modes corresponding to each wavevector $\mathbf{k}$. Since in the current work we consider a $2 \times 2 \times 2$ block of unit cells and sodalite possesses a cubic symmetry, there are only four independent wavevectors, $\mathbf{k} = [000]$, [100], [110] and [111], in our MD system. For reference, the dispersion relationships $\omega_{j\mathbf{k}}^h$ for sodalite for wavevectors $\mathbf{k}$ pointing in directions [100], [110] and [111] are shown in Figure 2. Normal modes accessible by the MD simulations

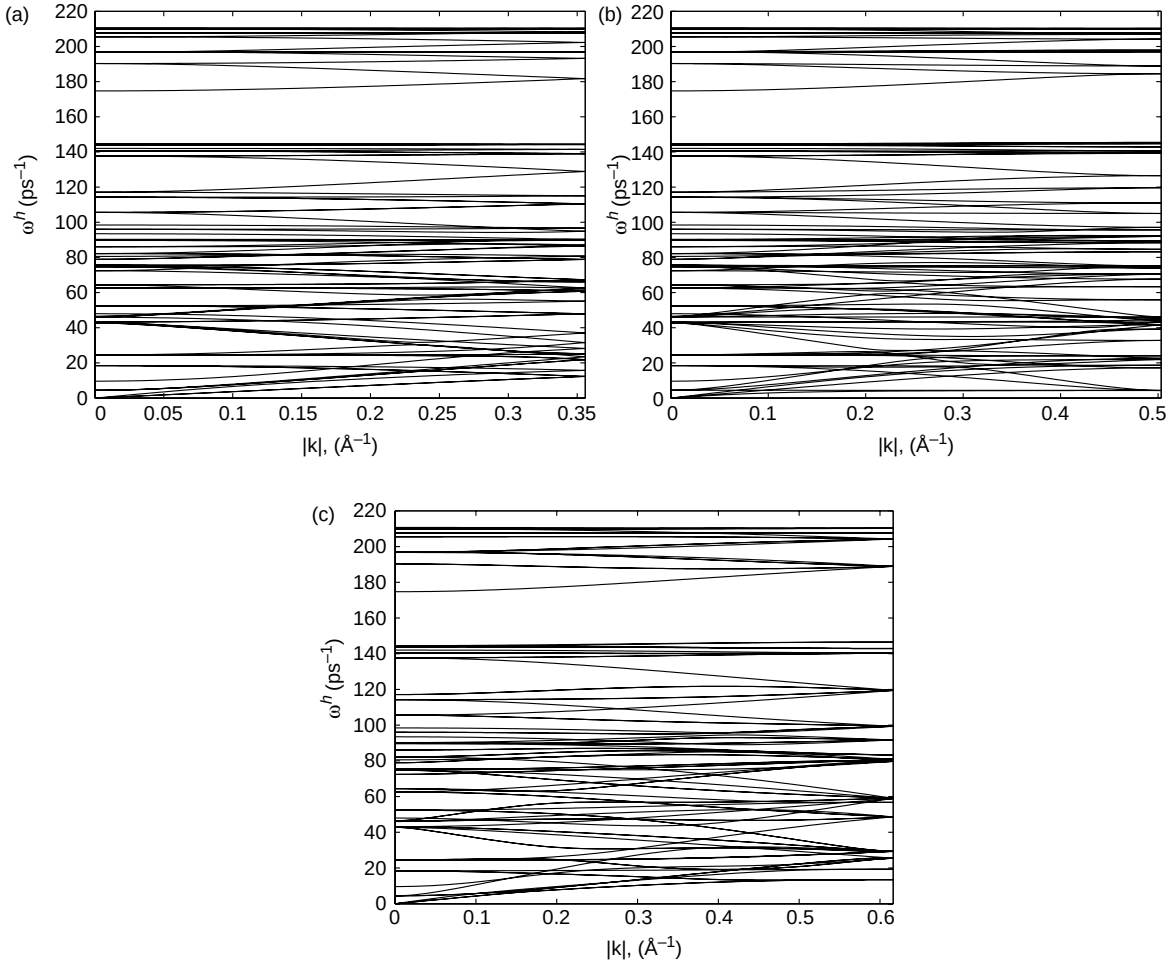

Figure 2. Dispersion relationships for sodalite in directions (a) $\mathbf{k} = [100]$, (b) $\mathbf{k} = [110]$ and (c) $\mathbf{k} = [111]$.

correspond to the smallest and the largest values of $|k|$ in each of these three plots.

In general, encapsulation of a sorbate inside a zeolite cage may affect the linearised lattice dynamics and lead to changes in the eigenvectors of the dynamical matrix, which would require one to use different normal modes in the analysis of zeolite lattice vibration in the presence of sorbates. However, this effect is significant only in the case of strong interaction between phonons and a sorbate located at an equilibrium adsorption site. This situation would occur if the sorbate were to fit tightly within a zeolite cage or if there were to be long-range electrostatic interactions between the sorbate and the zeolite lattice. It has been shown in [16] that coupling between the phonon modes and small electrically neutral sorbates, such as those considered in the current work, is negligible when the sorbates are located at adsorption sites inside sodalite cages. For these systems, the sorbate–phonon coupling becomes significant only when the sorbate approaches the zeolite wall. Therefore, the presence of the sorbates does not affect the dynamical matrix of the crystal.

The nonlinear effects of the sorbates, such as the change in phonon lifetime and the nonlinear corrections to the phonon frequency are analysed in the next two sections. The insensitivity of the harmonic approximation of the lattice dynamics to the sorbates considered in the current work allows us to use the normal modes of the sorbate-free zeolite to analyse the lattice dynamics in the presence of the sorbates. In the remainder of the paper, we use harmonic phonon frequencies $\omega^h_{j\mathbf{k}}$ to parameterise various plots of properties of individual modes. This allows us to consistently identify a phonon mode even if its frequency is changed upon addition of sorbates.

5. Nonlinear phonon and sorbate dynamics

Nonlinear phonon dynamics is usually modelled by the Boltzmann transport equation (BTE) [4]

$$\mathbf{v}_{j\mathbf{k}} \cdot \nabla T \frac{\partial n_{j\mathbf{k}}}{\partial T} = \left(\frac{\partial n_{j\mathbf{k}}}{\partial t} \right)_{\text{collision}}, \tag{12}$$

where T is the temperature and $\mathbf{v}_{j\mathbf{k}}$ and $n_{j\mathbf{k}}$ are the group velocity and the occupation number of the phonon mode $j\mathbf{k}$. The occupation number $n_{j\mathbf{k}}$ is proportional to the harmonic potential energy of the mode $j\mathbf{k}$ [23]. Phonon–phonon interactions due to lattice anharmonicity, defects and other factors are modelled by the collision integral in the right-hand side of Equation (12). Calculation of the collision integral in exact form is very challenging and it is usually approximated by various models, such as the single mode relaxation time (SMRT) approximation,

$$\left(\frac{\partial n_{j\mathbf{k}}}{\partial t}\right)_{\text{collision}} = \frac{n_{j\mathbf{k}}^{\text{eq}} - n_{j\mathbf{k}}}{\tau_{j\mathbf{k}}}. \tag{13}$$

Here, $n_{j\mathbf{k}}^{\text{eq}}$ is the equilibrium phonon distribution and $\tau_{j\mathbf{k}}$ is the relaxation time of the phonon mode $j\mathbf{k}$, which is assumed to coincide with the phonon lifetime. The relaxation time can be estimated from MD simulations by computing relaxation times of the occupation number [23] or the harmonic energy (11) of the normal mode [24].

The analysis of the phonon dynamics based on BTE approach has several drawbacks. The relaxation time approximation may not be adequate to model phonon dynamics in complex materials. Although SMRT approximation (13) can be extended to account for multiple relaxation times due to different phonon scattering mechanisms, these extensions require the phonon autocorrelation function to be a sum of multiple exponentials. However, as will be shown below, some of the sodalite phonon modes do not satisfy this requirement. In this case, a straightforward extension of the relaxation time model does not seem to be possible. In addition, the relaxation time approximation may not be appropriate to account for phonon–sorbate interactions.

In order to attain more flexibility in modelling phonon dynamics, we choose an alternative model based on Langevin equation [25],

$$\ddot{Q}_{j\mathbf{k}} + \gamma_{j\mathbf{k}}\dot{Q}_{j\mathbf{k}} = -\left(\omega_{j\mathbf{k}}^{a}\right)^2 (Q_{j\mathbf{k}} - \langle Q_{j\mathbf{k}}\rangle) + \Gamma_{j\mathbf{k}}(t). \tag{14}$$

Here, $\langle Q_{j\mathbf{k}}\rangle$ is the mean value of the normal mode coordinate $Q_{j\mathbf{k}}$, which may differ from zero due to anharmonicity of the system, $\omega_{j\mathbf{k}}^{a}$ is the anharmonic frequency, $\gamma_{j\mathbf{k}}$ is the friction coefficient, and $\Gamma_{j\mathbf{k}}(t)$ is the random force with zero mean which is related to the friction coefficient by the fluctuation–dissipation theorem

$$\langle \Gamma_{j\mathbf{k}}(t)\Gamma_{j\mathbf{k}}(t+\tau) = 2k_B T \gamma_{j\mathbf{k}}\delta(\tau). \tag{15}$$

We assume that the deterministic force in this Langevin model is still harmonic and the anharmonicity of the oscillations can be adequately captured by shifts in the phonon frequency and average normal mode coordinates, as well as friction and stochastic forces.

The autocorrelation function of normal mode $Q_{j\mathbf{k}}$ satisfying Equation (14) is [26]

$$C_{j\mathbf{k}}(\tau) = \langle \delta Q_{j\mathbf{k}}(t)\delta Q_{j\mathbf{k}}^{*}(t+\tau)\rangle \,\alpha\, \mathrm{e}^{-\tau/\tau_{j\mathbf{k}}} \times \cos\tilde{\omega}_{j\mathbf{k}}(\tau + \phi_{j\mathbf{k}}). \tag{16}$$

Here,

$$\delta Q_{j\mathbf{k}} = Q_{j\mathbf{k}} - \langle Q_{j\mathbf{k}}\rangle, \tag{17}$$

is the deviation of the phonon mode from its average,

$$\tau_{j\mathbf{k}} = 2/\gamma_{j\mathbf{k}}, \tag{18}$$

is the phonon lifetime,

$$\tilde{\omega}_{j\mathbf{k}} = \sqrt{(\omega_{j\mathbf{k}}^{a})^2 - 1/\tau_{j\mathbf{k}}^2}, \tag{19}$$

is the apparent phonon frequency, and $\phi_{j\mathbf{k}}$ is a phase shift. Equation (16) demonstrates that similarly to BTE with SMRT approximation, the Langevin model (14) predicts an exponential decay of the normal mode autocorrelation function. However, the Langevin equation provides more flexibility and allows one to perform relatively simple adjustments of the model to fit observed phonon dynamics. This can be done by including an explicit anharmonic term into the equation or modifying statistics of the random force. For example, non-exponential behaviour of the autocorrelation function can be modelled by a non-Markovian random force [27].

Examples of phonon autocorrelation functions obtained from our MD simulations of sorbate-free sodalite are shown in Figure 3. Most of these functions, such as that shown in Figure 3(a), are in good agreement with Equation (16). However, some modes exhibit significant deviations from the predictions of this Markovian Langevin equation. Autocorrelation functions of all these non-Markovian modes are qualitatively similar to one of the autocorrelation functions shown in Figure 3(b)–(d). These modes possess secondary (slow) oscillations which are qualitatively similar to oscillations of the autocorrelation function of the energy of an entire sodalite cage observed by McGaughey and Kaviany [28]. These secondary oscillations were interpreted as corresponding to localisation of energy in sodalite cages. Our analysis of individual phonon modes shows that only a fraction of optical phonons modes possesses this secondary time-scale.

In the current work, we assume that the Markovian Langevin Equation (14) provides an adequate model for the phonon dynamics and leave development of its extensions to account for secondary oscillations to future studies. Therefore, the lifetimes and the frequencies of all modes are obtained by applying Equation (16) to analysis of their autocorrelation function.

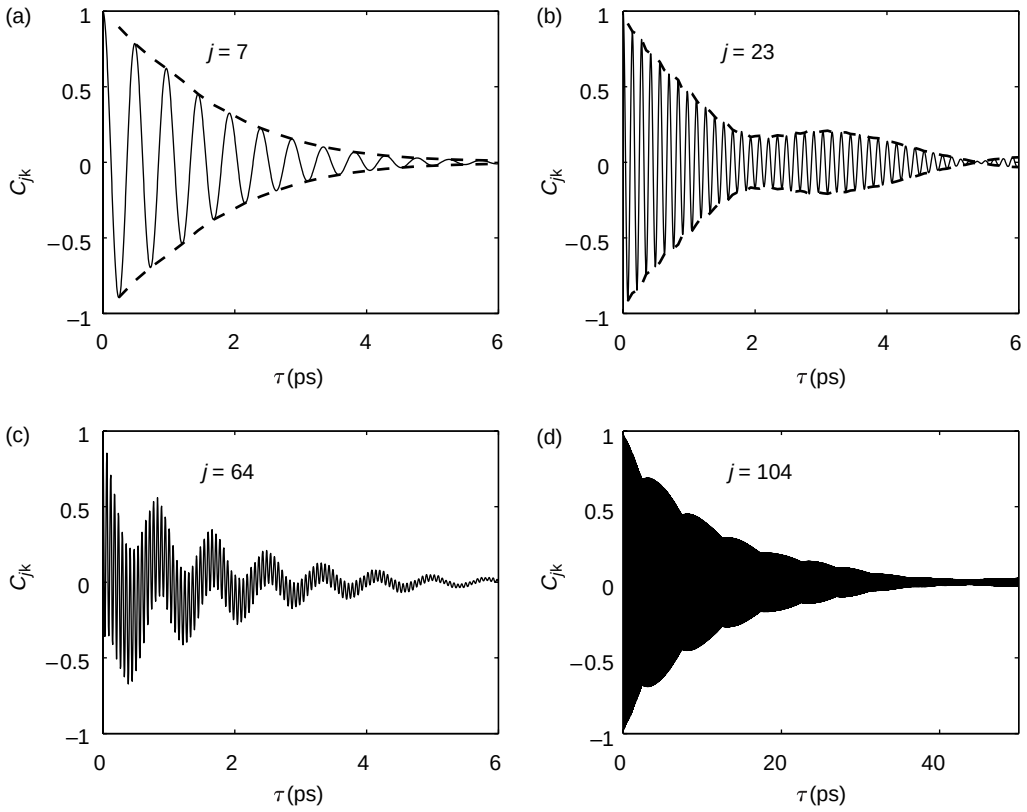

Figure 3. Examples of autocorrelation functions $C_{j\mathbf{k}}(\tau)$ of phonons in a sorbate-free sodalite crystal. The normal mode numbers j are shown in the corresponding plots; the wavevector is $\mathbf{k} = [000]$ in all four examples. In plots (a) and (b), envelopes $\pm E_{j\mathbf{k}}(\tau)$ of the autocorrelation functions are shown by dashed lines.

In particular, Equation (16) implies that the power spectrum $S_{j\mathbf{k}}(\omega)$ of the phonon mode $j\mathbf{k}$ attains its maximum at $\omega = \tilde{\omega}_{j\mathbf{k}}$. Therefore, we define the apparent frequency of vibration, $\tilde{\omega}_{j\mathbf{k}}$, as the location of the maximum of $S_{j\mathbf{k}}(\omega)$ for all modes, including those exhibiting significant deviations from Equation (16). Typical examples of power spectra of the normal modes are shown in Figure 4. We observe that for most modes, even those not satisfying the Langevin model (14), the maximum of $S_{j\mathbf{k}}$ corresponds to the highest frequency of oscillations which we associate with the apparent phonon frequency. In a few cases, such as that shown in Figure 4(c), the maximum of $S_{j\mathbf{k}}$ corresponds to slower secondary oscillations. In these cases, the apparent phonon frequency was defined as the frequency of a local maximum of $S_{j\mathbf{k}}(\omega)$ with the largest value of ω.

In order to estimate the lifetime of a phonon mode, we define an envelope $E_{j\mathbf{k}}(t)$ of its autocorrelation function $C_{j\mathbf{k}}(t)$ as a line connecting local maxima of $C_{j\mathbf{k}}(t)$, as shown by dashed lines in Figure 3(a),(b). The function $E_{j\mathbf{k}}$ is then fitted to an exponential. In the cases of non-exponential decay of $E_{j\mathbf{k}}$, the phonon lifetime is obtained by fitting its initial (quickly decaying) segment to an exponential.

Once the apparent phonon frequency $\tilde{\omega}_{j\mathbf{k}}$ and the lifetime $\tau_{j\mathbf{k}}$ are obtained, the anharmonic phonon frequency $\omega^a_{j\mathbf{k}}$ is computed from Equation (19). This equation is correct only for phonon normal modes that satisfy the Markovian Langevin equation (14). However, the difference between $\tilde{\omega}_{j\mathbf{k}}$ and $\omega^a_{j\mathbf{k}}$ is negligible if $\tilde{\omega}_{j\mathbf{k}} >> 1/\tau_{j\mathbf{k}}$. As will be shown in Section 6, phonon lifetimes range from 0.4 to 30 ps. Therefore, the correction of the apparent frequency (19) is significant only for phonons with very small frequencies. Our results indicate that dynamics of the low-frequency modes are in good agreement with the predictions of Equation (14) (Figure 3(a)). The correction of the apparent frequency is accurate for these modes. On the other hand, this correction is negligible for the high-frequency modes which do not satisfy the Markovian model (14).

Autocorrelation functions $C_{j\mathbf{k}}$ of a phonon mode $j\mathbf{k}$ in a sorbate-free sodalite and a sodalite containing sorbates are qualitatively similar for the same values of j and $\mathbf{k}$. This provides an additional confirmation that small neutral sorbates do no alter the phonon eigenmodes (see discussion at the end of Section 4). The sorbates affect such phonon properties as their lifetime and frequency. It will be shown in the next section that some of these

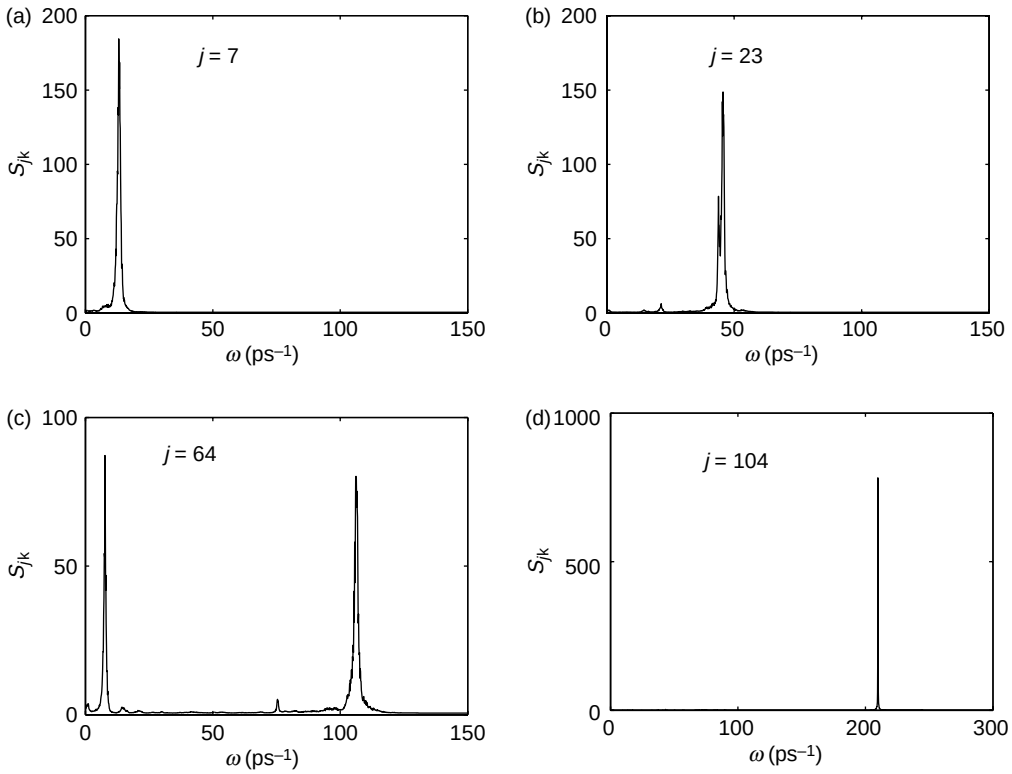

Figure 4. Power spectra $S_{j\mathbf{k}}(\omega)$ corresponding to the phonon autocorrelation functions shown in Figure 3. The normal mode numbers j are shown in the corresponding plots and the wavevector is $\mathbf{k} = [000]$ in all four examples.

changes, namely an increase of lifetime of some phonon modes, are qualitatively different from those expected from the simple phonon scattering picture. This implies that the sorbate dynamics is qualitatively different from that of point defects coupled to the lattice by a nearly harmonic potential. In fact, the sorbate dynamics is chaotic even in the absence of the thermal interaction with the lattice vibration. This is confirmed by the power spectra $S_V(\omega)$ of the sorbate velocities in the rigid zeolite shown in Figure 5. These power spectra are rather wide, implying chaotic sorbate dynamics due to strongly nonlinear interactions between the sorbates and the zeolite walls. The nonlinear effects are even stronger for systems with two sorbates per cage, as indicated by the wider sorbate velocity spectra in these systems.

6. Phonon statistics

Anharmonicity of lattice vibrations and sorbate–phonon interactions lead to non-zero mean values of some normal mode coordinates $Q_{j\mathbf{k}}$. The normal modes $Q_{j\mathbf{k}}$ with sufficiently large relative deviation of their mean from zero,

$$\Delta Q_{j\mathbf{k}} = \frac{\langle Q_{j\mathbf{k}} \rangle}{\sigma_{j\mathbf{k}}} \geq 0.04, \tag{20}$$

are listed in Table 3. In Equation (20), $\sigma_{j\mathbf{k}}$ denotes the standard deviation of the normal mode fluctuations.

In the sorbate-free lattice, modes $Q_{j\mathbf{k}}$ with $j = 7$ and 63 and $\mathbf{k} = [000]$ deviate from zero by 4 and 3 standard deviations, respectively. All other modes have much smaller deviations, $\Delta Q_{j\mathbf{k}} < 0.02$. Addition of one sorbate per cage essentially does not change the values of $\Delta Q_{j\mathbf{k}}$. However, addition of two sorbates per cage leads

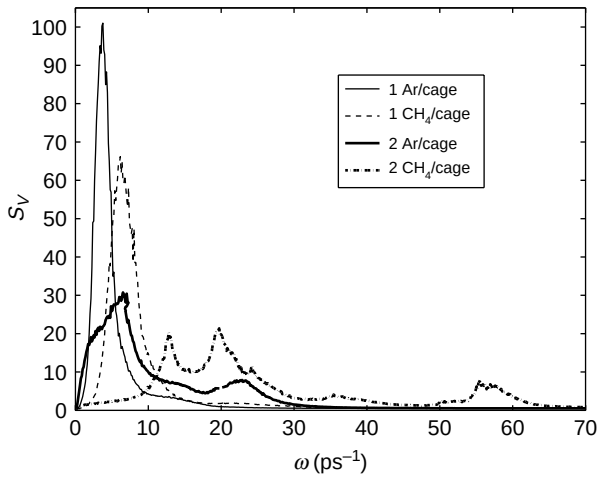

Figure 5. Power spectra $S_V(\omega)$ of sorbate velocities in rigid zeolite cages.

Table 3. Normalised averages of phonon amplitudes, $\Delta Q_{j\mathbf{k}} = \langle Q_{j\mathbf{k}} \rangle / \sigma_{j\mathbf{k}}$.

		$\Delta Q_{j\mathbf{k}}$					
			Sorbates/cage				
$j\mathbf{k}$	$\omega^h_{j\mathbf{k}}$ (ps^{-1})	Bare lattice	1 Ar	1 CH_4	1 Xe	2 Ar	2 CH_4
7 [000]	9.6	4.00	3.98	4.03	3.95	4.00	4.33
63 [000]	98.4	−3.14	−3.21	−3.18	−3.18	−3.23	−3.69
48 [000]	80.6	–	–	–	–	0.26	0.83
60 [000]	93.5	–	–	–	–	−0.048	−0.152
1 [110]	4.3	–	–	–	–	–	0.048
78 [000]	142.0	–	–	–	–	–	−0.043

Only modes with sufficiently large average deviations from zero, $\Delta Q_{j\mathbf{k}} \geq 0.04$, are shown. Normal modes are listed in the order of descending $\Delta Q_{j\mathbf{k}}$. Harmonic phonon frequencies $\omega^h_{j\mathbf{k}}$ corresponding to the listed modes are also shown.

to a substantial shift of average values of several additional modes, implying that the equilibrium lattice configuration slightly changes due to the presence of the sorbates. This change is larger in the case of 2 CH_4/cage. Addition of 2 CH/cage shifts averages of several normal modes away from zero as well as further increases $\Delta Q_{j\mathbf{k}}$ of the modes $j = 7$ and 63 ($\mathbf{k} = [000]$) that were already shifted in the sorbate-free lattice. Nevertheless, even the strongest sorbate effects on the mean normal coordinates seen in the case of 2 CH_4/cage are significantly weaker than effects of introduction of anharmonicity to a harmonic sodalite lattice.

It is interesting to note that all substantial shifts of $\langle Q_{j\mathbf{k}} \rangle$ take place for optical lattice modes with $\mathbf{k} = [000]$. The largest relative displacement of an acoustic mode is rather small ($\Delta Q_{j\mathbf{k}} = 0.048$) and is observed for mode $j = 1$, $\mathbf{k} = [110]$ when 2 CH_4/cage are added.

Phonon lifetimes $\tau_{j\mathbf{k}}$ in sorbate-free anharmonic lattice range from 0.4 to 30 ps, as shown in Figure 6. The modes with intermediate frequencies, $70\,ps^{-1} \leq \omega^h_{j\mathbf{k}} \leq 150\,ps^{-1}$, possess short lifetimes. The phonons with high frequencies, $\omega^h_{j\mathbf{k}} > 150\,ps^{-1}$, correspond mostly to fast vibrations of individual bonds. Interactions between these modes and other modes in the system are weak leading to large phonon lifetimes for the high-frequency modes. Some modes with low frequencies, $\omega^h_{j\mathbf{k}} < 70\,ps^{-1}$, also possess long lifetimes. However, most of the low-frequency modes possess relatively short lifetimes indicating that they are strongly coupled with other modes in the system.

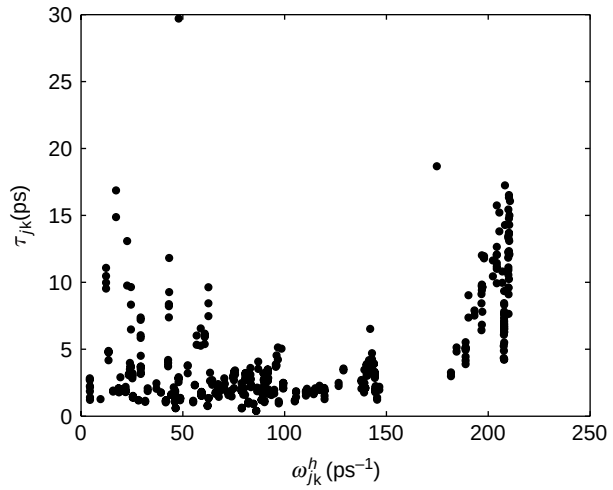

Figure 6. Phonon lifetimes $\tau_{j\mathbf{k}}$ in sorbate-free sodalite lattice.

For comparison, analysis of McGaughey and Kaviany [28] based on a decomposition of the heat current autocorrelation function predicts decay time for heat transfer associated with long-range acoustic modes in sodalite to be 1.67 ps. In addition, Greenstein et al. [10] have estimated phonon relaxation time in MFI zeolite to be 9.2 ps by fitting a theoretical expression to experimental thermal conductivity data. This estimate is based on an assumption that the relaxation time is the same for all phonon modes. Both of these estimations are within the range of the phonon lifetimes observed in the current work.

Relative changes of phonon lifetimes,

$$\delta\tau_{j\mathbf{k}} = \frac{\tau^s_{j\mathbf{k}} - \tau^a_{j\mathbf{k}}}{\tau^a_{j\mathbf{k}}}, \tag{21}$$

upon encapsulation of sorbates into the zeolite cages are shown in Figure 7. In Equation (21) and elsewhere in this paper superscript *s* refers to a property related to a zeolite with encapsulated sorbates. The distributions of $\delta\tau_{j\mathbf{k}}$ shown in Figure 7(a) are almost identical for all three systems with 1 sorbate/cage. These distributions are symmetric with respect to $\delta\tau = 0$, which implies that the phonon–sorbate interactions are equally likely to decrease as well as increase the phonon lifetime. The increase of the phonon lifetime contradicts a simple picture of phonon scattering by sorbates and implies that a more complex sorbate–phonon interaction is in play.

When two sorbates per cage are added to the system, the distribution of $\delta\tau_{j\mathbf{k}}$ becomes skewed towards average decrease of the phonon lifetime. This trend is especially

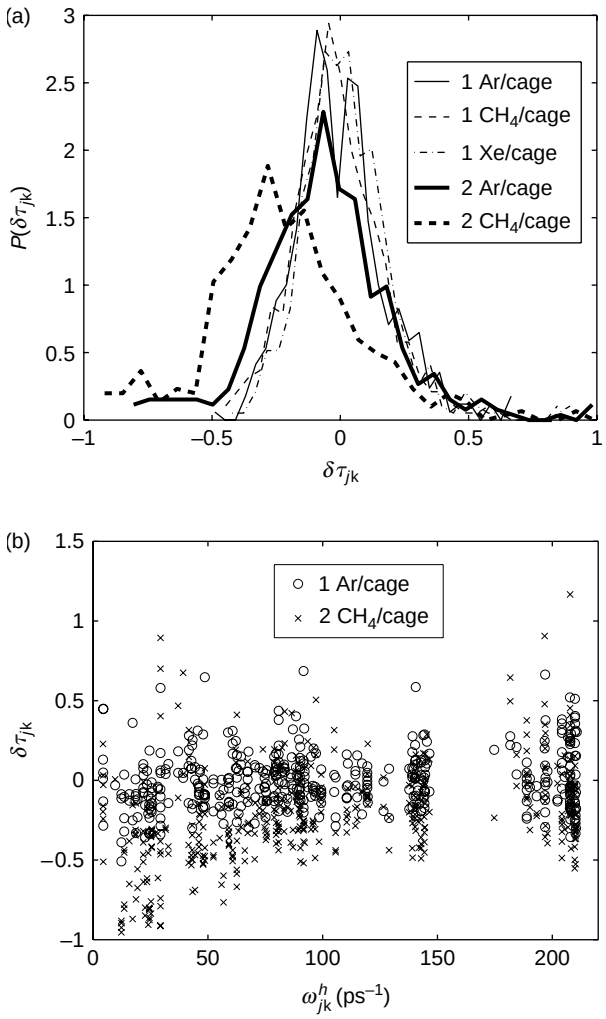

Figure 7. Effects of sorbates on phonon lifetimes: (a) distributions $P(\delta\tau_{j\mathbf{k}})$ of the relative differences $\delta\tau_{j\mathbf{k}}$ between the phonon lifetimes $\tau^s_{j\mathbf{k}}$ in sodalite with encapsulated sorbates and the phonon lifetimes $\tau^a_{j\mathbf{k}}$ in a sorbate-free sodalite and (b) relative changes $\delta\tau_{j\mathbf{k}}$ of lifetimes of individual modes $j\mathbf{k}$ for the cases of 1 Ar/cage and 2 CH/cage.

pronounced in the case of a larger sorbate, namely methane. This can be explained, in part, by a tighter fit of the sorbates within the cages leading to a smaller amplitude of the sorbate oscillations, which suggests more similarities between sorbates in these systems with point defects. However, as Figure 5 indicates, the sorbate dynamics in the 2 sorbate/cage systems is more chaotic than in the 1 sorbate/cage systems. Therefore, the analogy between the 2 sorbates/cage systems and crystals with point defects is not complete. Indeed, Figure 7 shows that some of the phonon modes in the 2 sorbates/cage systems undergo a significant (on the order of 100%) increase of their lifetime and hence the scattering model is still not applicable to this case.

In order to assess which of the modes undergo increase or decrease of their lifetime, in Figure 7(b) we plot $\delta\tau_{j\mathbf{k}}$ for every phonon mode. For clarity, only two extreme cases are shown: 1 Ar/cage and 2 CH_4/cage. For 1 Ar/cage, the changes of phonon lifetimes are evenly distributed among different frequencies. In the 2 CH_4/cage system, the modes lying in the small and large frequency regions experience, on average, larger change of their lifetimes than the modes with intermediate frequencies.

Effects of anharmonicity on the phonon frequency in a sorbate-free sodalite crystal are summarised in Figure 8 which shows relative differences,

$$\delta\omega_{j\mathbf{k}} = \frac{\omega^a_{j\mathbf{k}} - \omega^h_{j\mathbf{k}}}{\omega^h_{j\mathbf{k}}}, \tag{22}$$

between the anharmonic and harmonic phonon frequencies. With few exceptions, anharmonicity leads to an increase of the phonon frequency. This increase is especially large for low-frequency modes.

Addition of sorbates to zeolite cages typically leads to a further frequency increase, as can be seen from the relative differences

$$\delta\omega^s_{j\mathbf{k}} = \frac{\omega^s_{j\mathbf{k}} - \omega^a_{j\mathbf{k}}}{\omega^a_{j\mathbf{k}}}, \tag{23}$$

between phonon frequencies in sodalite with encapsulated sorbates ($\omega^s_{j\mathbf{k}}$) and in the sorbate-free sodalite ($\omega^a_{j\mathbf{k}}$) (Figure 9). The frequency changes $\delta\omega^s_{j\mathbf{k}}$ are substantially larger when more than one sorbate per cage is introduced. Similarly to $\delta\omega_{j\mathbf{k}}$, $\delta\omega^s_{j\mathbf{k}}$ tends to increase

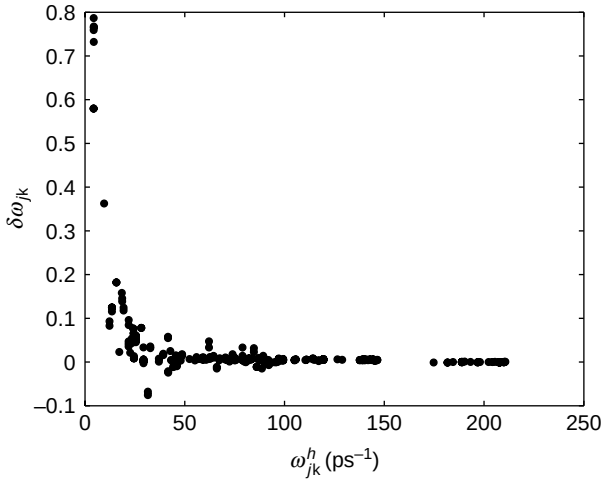

Figure 8. Relative differences $\delta\omega_{j\mathbf{k}}$ between the anharmonic ($\omega^a_{j\mathbf{k}}$) and harmonic ($\omega^h_{j\mathbf{k}}$) frequencies in a sorbate-free sodalite crystal.

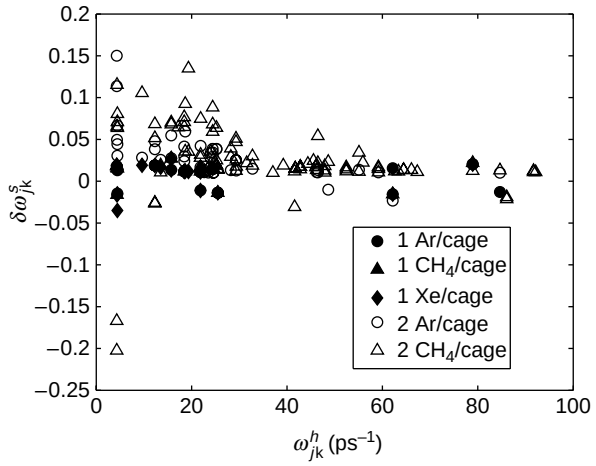

Figure 9. Relative differences $\delta\omega^s_{j\mathbf{k}}$ between phonon frequencies in sodalite with encapsulated sorbates ($\omega^s_{j\mathbf{k}}$) and in the sorbate-free sodalite ($\omega^a_{j\mathbf{k}}$). For clarity, only $\delta\omega^s_{j\mathbf{k}}$ with magnitudes greater than 10^{-2} are shown.

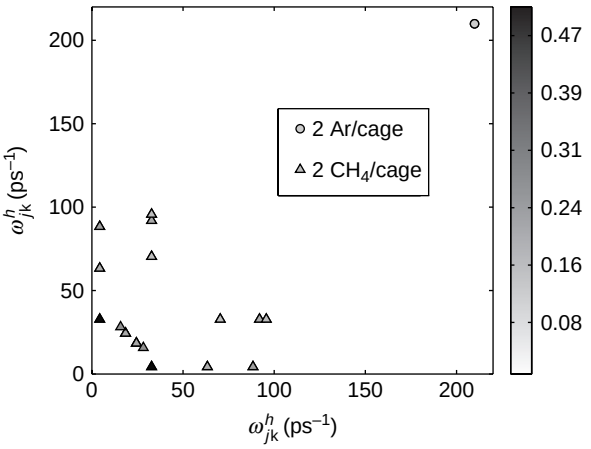

Figure 11. Effect of sorbates on phonon–phonon correlations. Only those pairs ($j\mathbf{k}$, $j'\mathbf{k}'$) are shown for which addition of sorbates creates a correlation with coefficient greater than 0.1 or changes the magnitude of an existing correlation by more than 0.1. Magnitudes of the changed correlation coefficients are indicated by colour.

with the decrease of the phonon frequency. However, the changes of phonon frequencies due to addition of sorbates are smaller than the changes due to introduction of anharmonicity to a sorbate-free harmonic lattice.

Up to this point, we have investigated effects of anharmonicity and sorbate–phonon interactions on individual phonon modes. To complete the picture, we now consider correlations between different phonon modes. It is expected that this information will be helpful in developing a more precise form of the Langevin model (14) for phonon dynamics since it will allow us to assess which phonons make dominant contributions to stochastic forces acting on each of the phonon modes. The magnitudes of the correlation coefficients

$$\rho(j\mathbf{k}, j'\mathbf{k}') = \left| \frac{\langle \delta Q_{j\mathbf{k}} \delta Q^*_{j'\mathbf{k}'} \rangle}{\sigma_{j\mathbf{k}} \sigma_{j'\mathbf{k}'}} \right|, \tag{24}$$

between modes $j\mathbf{k}$ and $j'\mathbf{k}'$ in a sorbate-free lattice are shown in Figure 10. For clarity, only correlations of magnitude exceeding 0.1 are plotted. Most correlation coefficients between individual phonons are rather weak. Correlations between low- and mid-frequency modes constitute a notable exceptions: some correlations of low-frequency modes with modes of frequency $\omega^h_{j\mathbf{k}} \approx 100\,\mathrm{ps}^{-1}$ have correlation coefficient as large as 0.5. These observations are consistent with the measured phonon lifetimes (Figure 6). Specifically, phonon–phonon correlations involving the high-frequency modes are very weak, which is manifested in long lifetimes of these modes. The modes with intermediate frequencies, $70\,\mathrm{ps}^{-1} \leq \omega^h_{j\mathbf{k}} \leq 150\,\mathrm{ps}^{-1}$, are strongly correlated with some of the low-frequency modes, which leads to small lifetime of these modes.

Effect of the sorbate presence on the phonon–phonon correlations is shown in Figure 11. Addition of a single sorbate per cage leads to relatively small changes in phonon–phonon correlations, with no phonon pairs with correlation coefficient greater than 0.1 being affected. Addition of 2 Ar/cage creates one new phonon–phonon correlation with magnitude slightly larger than 0.1. In contrast, addition of 2 CH_4/cage creates several strong correlations and magnifies some correlations which were present in the sorbate-free lattice. The largest changes of the correlation coefficients upon addition of 2 CH_4/cage

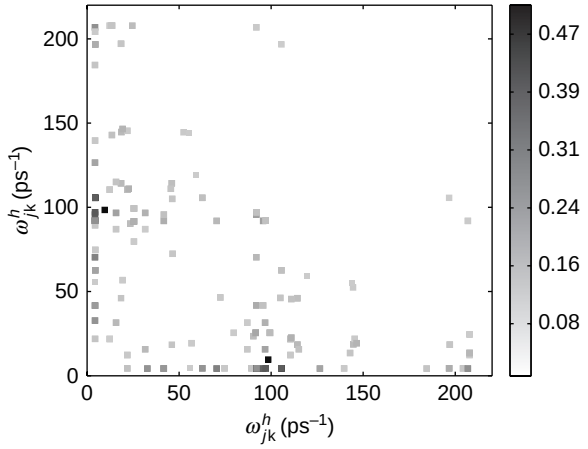

Figure 10. Magnitudes of correlation coefficients $\rho(j\mathbf{k}, j'\mathbf{k}')$ between phonon modes $j\mathbf{k}$ and $j'\mathbf{k}'$ in a sorbate-free sodalite crystal. Darker symbols correspond to stronger correlations. For clarity, correlation coefficients for $j\mathbf{k} = j'\mathbf{k}'$ are not shown and only correlations of magnitude greater than 0.1 are plotted.

are between the low-frequency acoustic modes with wavevector $\mathbf{k} = [110]$ and other phonons. The change of the correlation coefficient in these cases is $\Delta\rho \approx 0.27$.

7. Conclusions

We have investigated phonon dynamics in sodalite for five different sorbate–zeolite systems: 1 Ar/cage, 1 CH_4/cage, 1 Xe/cage, 2 Ar/cage and 2 CH_4/cage, as well as a sorbate-free zeolite. We have observed that the Markovian Lanvegin equation (14) provides an adequate model for dynamics of most of the phonon modes. However, dynamics of some phonon modes does not agree with predictions of Equation (14). These modes exhibit secondary oscillations (Figure 3(b)–(d)) which are most likely related to the total energy fluctuations inside a single sodalite cage [28].

Encapsulation of sorbates in zeolite cages does not lead to qualitative changes of phonon dynamics, as can be concluded from phonon autocorrelation functions. However, depending on the type and number of sorbates inside sodalite cage, some or all of the following aspects of phonon dynamics are changed: (i) the mean values of the normal mode coordinates, (ii) phonon lifetimes, (iii) phonon frequencies and (iv) phonon–phonon correlations. The largest changes of phonon dynamics are observed upon encapsulation of two methane molecules per sodalite cage.

The strongest effect of all considered sorbates on lattice dynamics is a significant change of the phonon lifetimes. From the scattering picture of phonon–sorbate interactions it is expected that these interactions will decrease phonon lifetimes. However, we observe that encapsulation of sorbates leads to an increase of lifetimes of a large fraction of phonons. Therefore, development of a more detailed model is necessary to understand the complex nonlinear sorbate–phonon interactions.

Acknowledgements

This research was supported by the University of Florida. The authors acknowledge stimulating discussions with Professors S. Nair and S. Graham.

References

[1] M. Tatlier and A. Erdem-Senatalar, *The performance analysis of a solar adsorption heat pump utilizing zeolite coatings on metal supports*, Chem. Eng. Commun. 180 (2000), p. 169.
[2] J.M. Gordon et al., *The electro-adsorption chiller: a miniaturized cooling cycle with applications to micro-electronics*, Int. J. Refrigeration – Revue Internationale Du Froid 25 (2002), p. 1025.
[3] Y. Hudiono et al., *Effects of composition and phonon scattering mechanisms on thermal transport in MFI zeolite films*, J. Appl. Phys. 102 (2007), 053523.
[4] G.P. Srivastava, *The Physics of Phonons*, Adam Hilger, Bristol, 1990.
[5] T.R. Forester and W. Smith, *Bluemoon simulations of benzene in silicalite-1. Predictions of free energies and diffusion coefficients*, J. Chem. Soc. Faraday Trans. 93 (1997), p. 3249.
[6] D.I. Kopelevich and H.-C. Chang, *Diffusion of inert gases in silica sodalite: importance of lattice flexibility*, J. Chem. Phys. 115 (2001), p. 9519.
[7] S. Turaga and S.M. Auerbach, *Calculating free energies for diffusion in tight-fitting zeolite-guest systems: Local normal-mode Monte Carlo*, J. Chem. Phys. 118 (2003), p. 6512.
[8] F. Jousse, D.P. Vercauteren, and S.M. Auerbach, *How does benzene in NaY zeolite couple to the framework vibrations?* J. Phys. Chem. B 104 (2000), p. 8768.
[9] V.V. Murashov, *Thermal conductivity of model zeolites: molecular dynamics simulation study*, J. Phys.: Condens. Matter 11 (1999), p. 1261.
[10] A.M. Greenstein et al., *Thermal properties and lattice dynamics of polycrystalline MFI zeolite films*, Nano. Micro. Thermophys. Eng. 10 (2006), p. 321.
[11] G.S. Nolas et al., *The effect of rare-earth filling on the lattice thermal conductivity of skutterudites*, J. Appl. Phys. 79 (1996), p. 4002.
[12] G.P. Meisner et al., *Structure and lattice thermal conductivity of fractionally filled skutterudites: solid solutions of fully filled and unfilled end members*, Phys. Rev. Lett. 80 (1998), p. 3551.
[13] J. Dong, O.F. Sankey, and C.W. Myles, *Theoretical study of the lattice thermal conductivity in Ge framework semiconductors*, Phys. Rev. Lett. 86 (2001), p. 2361.
[14] R. Tsekov and E. Ruckenstein, *Stochastic dynamics of a subsystem interacting with a solid body with application to diffusive processes in solids*, J. Chem. Phys. 100 (1994), p. 1450.
[15] P. Demontis and G.B. Suffritti, *Structure and dynamics of zeolites investigated by molecular dynamics*, Chem. Rev. 97 (1997), p. 2845.
[16] D.I. Kopelevich and H.-C. Chang, *Does lattice vibration drive diffusion in zeolites?* J. Chem. Phys. 114 (2001), p. 3776.
[17] J.W. Richardson, et al., *Conformation of ethylene-glycol and phase-change in silica sodalite*, J. Phys. Chem. 92 (1988), p. 243.
[18] K. Knorr et al., *High-pressure study on dioxolane silica sodalite $(C_3H_6O_2)_2[Si_{12}O_{24}]$ – neutron and X-ray powder diffraction experiments*, Solid State Commun. 113 (2000), p. 503.
[19] J.B. Nicholas et al., *Molecular modeling of zeolite structure. 2. Structure and dynamics of silica sodalite and silicate force-field*, J. Am. Chem. Soc. 113 (1991), p. 4792.
[20] A.V. Kiselev, A.A. Lopatkin, and A.A. Shulga, *Molecular statistical calculation of gas adsorption by silicalite*, Zeolites 5 (1985), p. 261.
[21] H.J.C. Berendsen et al., *Molecular dynamics with coupling to an external bath*, J. Chem. Phys. 81 (1984), p. 3684.
[22] A.A. Maradudin et al. *Theory of Lattice Dynamics in the Harmonic Approximation*, Academic Press, New York, 1971.
[23] A.J.C. Ladd, B. Moran, and W.G. Hoover, *Lattice thermal conductivity: a comparison of molecular dynamics and anharmonic lattice dynamics*, Phys. Rev. B 34 (1986), p. 5058.
[24] A.J.H. McGaughey and M. Kaviany, *Quantitative validation of the Boltzmann transport equation phonon thermal conductivity model under the single-mode relaxation time approximation*, Phys. Rev. B 69 (2004), 094303.
[25] S. Lepri, R. Livi, and A. Politi, *Thermal conduction in classical low-dimensional lattices*, Phys. Rep. 377 (2003), p. 1.
[26] G.W. Gardiner, *Handbook of Stochastic Methods for Physics, Chemistry, and the Natural Sciences*, Springer-Verlag, Berlin, 1983.
[27] J. Łuczka, *Non-Markovian stochastic processes: Colored noise*, Chaos 15 (2005), 026107.
[28] A.J.H. McGaughey and M. Kaviany, *Thermal conductivity decomposition and analysis using molecular dynamic simulations. Part II. Complex silica structures*, Int. J. Heat Mass Transfer 47 (2004), p. 1799.

[29] S. El Amrani, F. Vigné, and B. Bigot, *Self-diffusion of rare-gases in silicalite studied by molecular dynamics*, J. Phys. Chem. 96 (1992), p. 9417.

[30] D. Keffer, A.V. McCormick, and H.T. Davis, *Unidirectional and single-file diffusion in $AlPO_4$-5: molecular dynamics investigations*, Mol. Phys. 87 (1996), p. 367.

[31] S.J. Goodbody et al., *Molecular simulation of methane and butane in silicalite*, J. Chem. Soc. Faraday Trans. 87 (1991), p. 1951.

[32] R.L. June, A.T. Bell, and D.N. Theodorou, *Transition-state studies of xenon and SF_6 diffusion in silicalite*, J. Phys. Chem. 95 (1991), p. 8866.